Numerical Simulations for Life Assessments of the BaO and LaB_6 Cathode Options in the Hall Effect Rocket with Magnetic Shielding (HERMeS)

IEPC-2017-152

Presented at the 35th International Electric Propulsion Conference
Georgia Institute of Technology • Atlanta, Georgia • USA
October 8 – 12, 2017

Alejandro Lopez Ortega[1], Ioannis G. Mikellides[2] and Dan M. Goebel[3]
Jet Propulsion Laboratory, California Institute of Technology, Pasadena, CA, 91109, USA

Abstract: Two cathode technologies have been considered for the Hall-Effect Rocket with Magnetic Shielding (HERMeS) that are distinguished mainly by the emitter material they employ, namely LaB_6 and BaO. We present the results of numerical simulations of these two cathodes with the main objective to assess possible failures due to depletion/vaporization of the emitter material and erosion of the cathode electrodes. Design specifications for the HERMeS cathode call for 23 kh of operation that must be demonstrated with a 50% margin. The numerical simulations have been performed mainly with the Orificed Cathode 2D (OrCa2D) code. To assess the contribution of thruster ions to keeper erosion, simulations with Hall2De also have been performed since OrCa2D does not account for these ions. The OrCa2D results are first compared with internal probe measurements and emitter temperature data. We find that the expected emitter depletion rates and erosion rates of the orifice plate are well within the acceptable margins for preventing failure of the cathodes for all conditions of the required operating envelope. However, we also find that erosion of the keeper electrode due to ions generated inside the acceleration channel of the thruster or in the thruster plume is significant enough to warrant enlargement of the keeper thickness. It is also recommended that the keeper orifice exit plane be located upstream of the pole cover in a way that the latter provides some shielding of the keeper surface.

Nomenclature

$B_{r,max}$	=	maximum magnitude of the magnetic field along the centerline of the thruster channel
ε	=	erosion rate
h_{em}	=	emitter thickness
j_i	=	ion current density
K_i	=	ion energy
L_{em}	=	emitter length
t_{em}	=	emitter lifetime
T_{em}	=	emitter temperature
Y	=	sputtering yield
z	=	axial coordinate

[1] Member of the Technical Staff, Electric Propulsion Group, alejandro.lopez.ortega@jpl.nasa.gov.
[2] Principal Engineer, Electric Propulsion Group, ioannis.g.mikellides@jpl.nasa.gov.
[3] Senior Research Scientist, Propulsion, Thermal and Materials Engineering, dan.m.goebel@jpl.nasa.gov.

I. Introduction

NASA has been developing the Hall Effect Rocket with Magnetic Shielding (HERMeS) [1], a 12.5 kW-class Hall thruster that was the principal component of the Ion Propulsion System (IPS) for the Asteroid Robotic Redirect Mission (ARRM) [2-4]. Even though the ARRM concept has been officially canceled, the IPS is still under development through the Advanced Electric Propulsion System (AEPS) contract with Aerojet Rocketdyne and work conducted at NASA Glenn Research Center (GRC) and Jet Propulsion Laboratory (JPL) to provide insight/oversight and testing support of the contract as well as risk reduction and life qualification activities [5-6]. NASA has fabricated three Technology Development Unit (TDU) thrusters devoted to testing and Aerojet-Rocketdyne is currently working on the Engineering Development Unit (EDU). The design specifications for the HERMeS thruster called for 23 kh of operation of the propulsion system that must be demonstrated with a 50% margin. A centrally-mounted hollow cathode [7] is used as the primary electron source for the thruster. For HERMeS, two cathode emitters have been proposed, namely Barium Oxide (BaO) and Lanthanum Hexaboride (LaB_6). BaO has a lower work function than LaB_6, thus typically operating at a lower temperature for the same discharge current. On the other hand, BaO cathodes are subject to contamination while LaB_6 are orders of magnitude less sensitive to impurities. Both materials are capable of providing long life in thruster applications due to the relatively low depletion/evaporation rate. Recently, the project has selected the BaO version of the cathode to be included in the EDU for a variety of reasons, but chiefly since the aggressive development schedule for AEPS made selecting the BaO cathode a lower risk approach, due to its higher flight heritage in the United States.

Consistent with JPL Design Principles for the service life qualification of electric thrusters, the plan to qualify the EDU thruster has been to perform a 23-kh wear test and establish the 50% margin (additional 11.5 kh) through analysis that includes physics-based modeling and simulation (M&S). The M&S activities would also support the wear test by providing physics insight into the test observations and by simulating operating conditions that could not be assessed fully during the wear test. The JPL code Orificed Cathode 2D (OrCa2D), whose development began in mid-2000 [8-13], is used to simulate both the BaO and LaB_6 cathode designs. As will be shown in Section II, internal measurements of the plasma density, plasma potential, and emitter temperature are used for comparisons with numerical results obtained using OrCa2D. In particular, we focus our attention on three processes that have been historically identified as potential failure mechanisms. The first mechanism is the depletion or evaporation of the emitter material, the rate of which increases with emitter temperature. The second mechanism is orifice plate erosion [10,12,14]. Hollow cathode tubes typically end at a plate with an orifice whose radius is smaller than that of the tube. If the orifice is eroded significantly, the cathode may enter "plume mode," an unfavorably unstable mode of operation characterized by large global oscillations in the discharge and enhanced erosion rates. The third failure mechanism in hollow cathodes is the erosion of the cathode keeper [14-15]. The principal cause of keeper erosion has been identified as the sputtering by energetic ions. Energetic ions in the cathode plume are produced if the cathode operates in plume mode and/or if electron extraction occurs at high enough speeds to excite ion acoustic waves [10,16-17]. Thus, keeper erosion is prevented by employing materials with lower sputtering yield and by operating the cathode under conditions that eliminate or minimize the production of energetic (cathode) ions.

This article is organized as follows. Section II provides a short description of OrCa2D. Section III presents the comparison between OrCa2D results and internal probe measurements performed during tests. In Section IV, we summarize our findings for each of the possible failure mechanisms. Concluding remarks are provided in Section V.

II. Description of the OrCa2D code

The physics models and numerical methods in OrCa2D have been described in detail in [8-13,18-19] and will only be described briefly here. OrCa2D solves conservation laws for three species present in a partially ionized gas: electrons, singly charged xenon ions, and xenon neutrals. A time-splitting method in which all the equations are solved consecutively at every time-step is employed. Inside the cathode, the Navier-Stokes equations for neutral xenon are solved using an implicit backward Euler scheme, which includes the viscous terms. It has been shown that the flow of neutrals transitions from a low to a high Knudsen number downstream of the cathode orifice. Thus, a fluid

approximation is not applicable in the cathode plume. Free molecular flow, in which neutrals move in straight paths, is assumed downstream of an axial location, typically chosen to be in the cathode orifice where the Knudsen number approaches unity. Mass and momentum continuity is preserved across the transition boundary. The Euler equations for mass and momentum of xenon ions are solved in the entire computational domain. The presence of ion momentum terms was recently included to account for the increased ion densities and currents in high-current cathodes. The effects of ionization, charge exchange and electron-ion collisions are considered in the equations and modeled as source or drag terms. Finally, the plasma parameters for electrons are determined from the solution of the electron energy equation and the combination of the current conservation equation with the vector form of Ohm's law. As confirmed by several results of OrCa2D simulations having been validated by plasma measurements [8-11,13,20], the largely collisional plasma inside most electric propulsion hollow cathodes lends itself to a continuum description of the conservation laws. The near-plume region of these devices however has proven more difficult to capture accurately. The first efforts to model the plume with OrCa2D revealed that electron resistivity due to classical collisions are orders of magnitude too low to explain the measured plasma parameters. Mikellides et al. [11] postulated that the presence of only classical resistivity in the plume of a hollow cathode was insufficient to explain the rise of the plasma potential and electron temperature measured downstream of the orifice of a cathode operating at 25 A. It was also pointed out in [8,20] by means of numerical simulations and analysis of the same cathode that the conditions for growth of ion-acoustic turbulence (IAT) [21-23] existed downstream of the orifice exit, and that when an idealized anomalous resistivity model for the electrons subjected to IAT was included the agreement with the measurements near the orifice improved significantly. Thus, the resistivity in Ohm's law is determined as a function of the classical collision frequencies (i.e., electron-ion and electron-neutral) and the anomalous collision frequency that models the effect of the IAT on the electron transport. The kinetic-based model that allows for the computation of the anomalous collision frequency requires solving a continuity equation for the amount of energy carried by the waves present in the turbulence and was presented in [18,19].

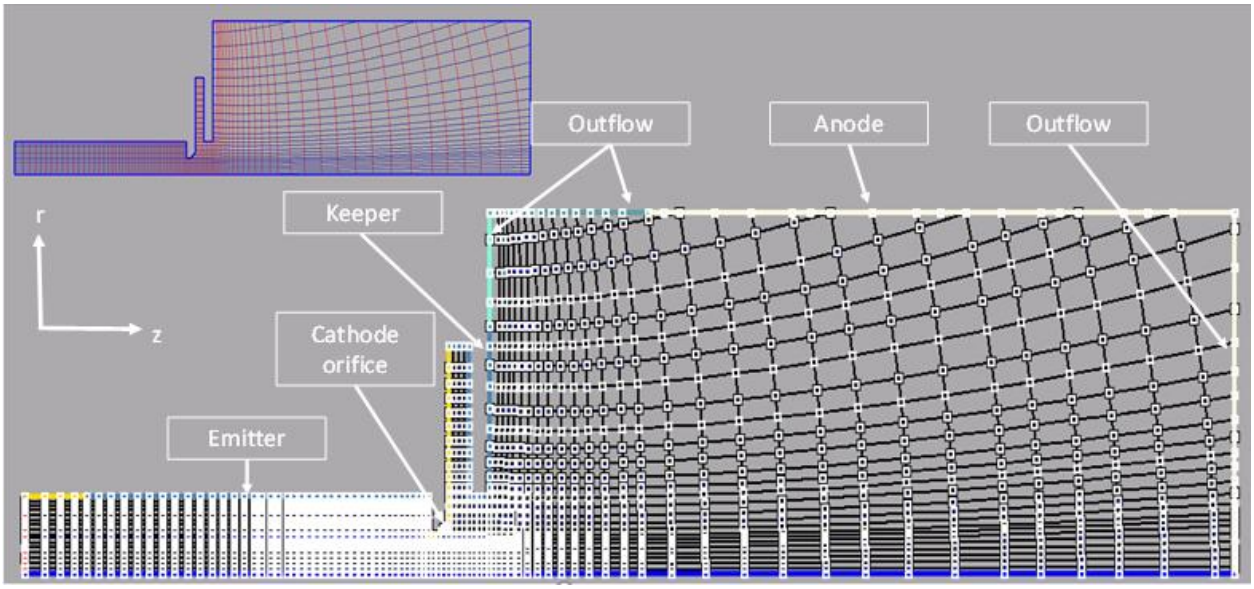

Figure 1. OrCa2D computational domain and mesh pointing to the different boundary conditions. The mesh in the cathode interior is rectilinear and a magnetic-field-aligned mesh (MFAM) is used for the plume.

The computational domain (Fig. 1) comprises the interior of the cathode tube and a considerable section of the plume, including the collecting surface of the anode. The anode dimensions are the same as those of the anode used in cathode tests, since it is known that modification of the anode geometry can lead to changes in the discharge voltage. Thus, the computational domain is designed in a way such that it can replicate the exact conditions at which a cathode test was run in the laboratory. Since a magnetic-field-aligned mesh (MFAM) [25-26] simplifies the solution of Ohm's law, the computational mesh can be made aligned to an applied external magnetic field if one existed in the laboratory test. Though the anode geometry in Fig. 1 is as shown for the purpose of emulating the specific arrangement in the HERMeS cathode tests, in principle, any 2-D axisymmetric geometry can be simulated by OrCa2D.

Boundary conditions are imposed at each surface and at the outflow. Boundary conditions for a conductor surface are used at the emitter, orifice, keeper, and anode. These conditions assume an infinitesimally small sheath that can be modeled as one-dimensional. In addition, the total electron current from the emitter is the difference between the emitted and absorbed current. The emitted current is determined by the Richardson-Dursham [27] emission equation and accounts for the Schottky effect [8]. At the keeper electrode where the plasma potential can be either below or above the keeper voltage when current is collected, the boundary conditions there account self-consistently for the transition from an ion-attracting to an ion–repelling sheath [28]. In OrCa2D the emitter temperature distribution along the emitter surface is specified either by direct measurements of the temperature, or indirectly based on measurements of plasma parameters in the interior of the cathode tube.

III. Comparison of OrCa2D solutions with experimental measurements

HERMeS operates at a nominal discharge current of 20.8 A and discharge voltages between 300 and 600 V. In addition, there exists a requirement for a low power condition with a discharge current of 9 A and discharge voltage of 300 V. The magnetic field can be adjusted between values along the channel centerline ($B_{r,max}$) that range between +/-25% of the nominal $B_{r,max}$. The cathode mass flow rate is nominally 7% of the anode mass flow rate but may be adjusted for operation at 5% and 9% of the anode mass flow rate. The anode mass flow rate exhibits minor variations between the 300 V and 600 V conditions [29] (19.52 mg/s at 300 V and 20.72 mg/s at 600 V). Thus, we can simplify the extent of our parametric study by computing the cathode mass flow rate for the 5% condition using the minimum anode mass flow rate (19.52 mg/s). This yields a cathode mass flow rate of 0.98 mg/s (10.57 sccm) and using the maximum anode mass flow rate (20.72 mg/s) for the 7% and 9% conditions (cathode mass flow rate of 1.4 mg/s (14.8 sccm) and 1.9 mg/s (19.0 sccm), respectively). Due to the presence of discharge current oscillations in the Hall thruster, it is also necessary to show that operation of the cathode at values above 20.8 A does not lead to detrimental life expectancy. We therefore conducted simulations with cathode currents of 23 and 25 A. Internal plasma measurements do not exist for the complete range of parameters in our study. We consequently adopt a set of rules to extrapolate validated results to other operating conditions:

- Since the Hall parameter inside the cathode is very low, internal plasma measurements do not significantly change in the presence of an external magnetic field or when the magnitude of the latter is modified. Thus, we will use the same set of measurements to compare results at different magnetic field intensities.
- We have found that emitter temperature profiles and plasma measurements are not significantly affected by changes in the mass flow rate [30, 31]. Thus, we may use the same emitter temperature profile for different mass flow rates if the discharge current is the same.
- If measurements are not available for a particular operating condition, we make use of the closest operating condition that has been validated and iterate on the maximum value of the emitter temperature without changing its spatial distribution (i.e., we add a constant to the emitter temperature profile)

A. Comparison between numerical results and experimental measurements in the LaB_6 cathode

Two LaB_6 cathodes with the same geometry except for the orifice size (nominal orifice diameter and an orifice diameter that is 50% larger) were proposed as candidates for HERMeS. Direct emitter temperature measurements were taken for the cathode with the large orifice at a wide range of operating conditions [31]. However, no such measurements exist for the cathode with the nominal orifice. Internal probe measurements for a mass flow rate of 13.1 sccm (slightly lower the nominal value of 14.8 sccm) and 25 A of discharge current are available for both cathodes. Since we are required to conduct simulations at a slightly higher-than-nominal discharge current to demonstrate operation during Hall thruster oscillations, we can use the plasma measurements to compare against the numerical results for the operating condition of 1.4 mg/s (7% of mass flow rate, 14.8 sccm) and 25 A.

Figure 2 shows comparisons along the channel centerline between measurements and simulation for the plasma density, electron temperature, and plasma potential of the LaB_6 cathode with 50% larger-than-nominal orifice diameter. The entrance to the cathode orifice (facing the interior plasma) is at $z/L_{em}=0$ and z/L_{em} increases with distance from the orifice towards the cathode interior. The measured emitter temperature profile is also compared to the profile used in OrCa2D along the length of the emitter L_{em}. Uncertainty values for the measurements are in the range of 50% for the plasma density and 1-2 V for the electron temperature and plasma potential. The plasma density extracted from the simulations exhibits a profile that appears to be flatter than the measured profile. The plasma potential falls below the measured values (although only two values are available from the measurements making difficult to extrapolate any trends in the evolution of the potential along the axis). The comparison between

experiments and simulations can probably be improved within the uncertainty range of the emitter temperature measurements. There exists a typical error of 10 C in the thermocouple measurements of emitter temperatures. In addition, results at the midpoint of the emitter are considered more reliable than at its extremes. The latter is due to proximity to other components of the cathode potentially interfering with the measurements. For instance, lower emitter temperatures close to the upstream end of the emitter would yield computed plasma parameters more similar to the measurements. As shown in Fig. 2, the computed plasma potential is lower than the measurement at the upstream end of the emitter, which means that more electron current returns to the emitter in the numerical simulation. With a lower value of the emitter temperature used as simulation input, the emitted current decreases, which necessarily means that the plasma must adjust itself to keep the discharge current constant by lowering the return current. The latter is achieved to first approximation by increasing the plasma potential.

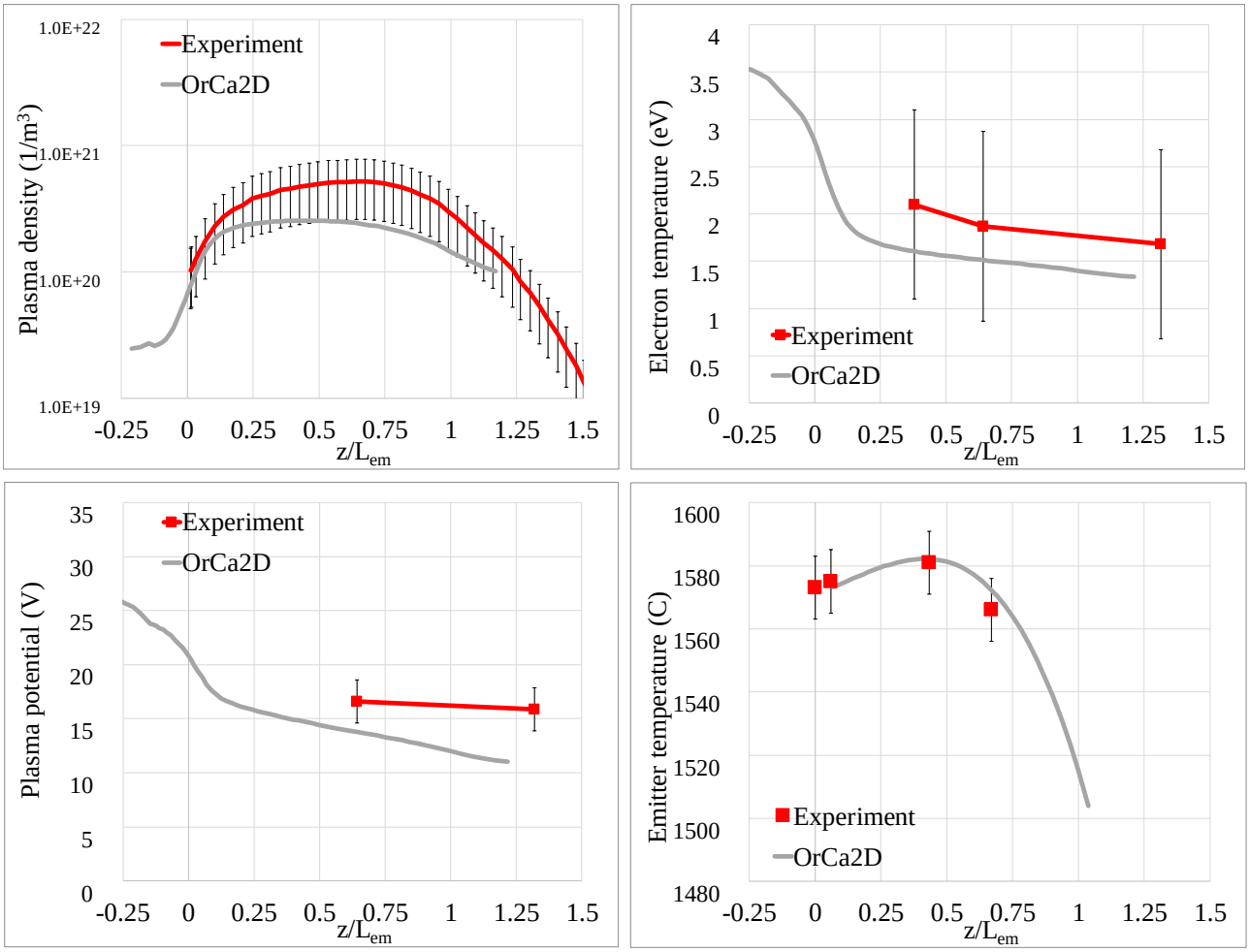

Figure 2. Comparison between internal plasma measurements and OrCa2D numerical simulation results along the cathode centerline and along the emitter surface for the LaB_6 cathode with 50% larger-than-nominal orifice diameter. Simulation run with mass flow rate of 14.8 sccm (compared to 13.1 sccm for the measurements) and discharge current of 25 A. Top-left: plasma density, top-right: electron temperature, bottom-left: plasma potential, bottom-right: emitter temperature.

For the LaB_6 cathode with nominal orifice diameter, emitter temperature measurements were attempted but the values yielded a current that was significantly below the discharge current, assuming thermionic emission only. This yields the maximum value of current achievable by the emitter since it does not account for electrons returning back to it due to the presence of the sheath. We therefore considered only the spatial variation of the measured temperature along the emitter to guide the profile used in the OrCa2D simulations. The maximum value of the temperature along this profile was then determined by iteration, until the operating discharge current was achieved. Figure 3 depicts the comparison between the simulation results and measurements at a discharge current of 25 A. The comparison between

simulations and measurements for the plasma density and electron temperature suggests agreement within the experimental uncertainty. As in the case of the cathode with the large orifice, the largest discrepancy between experiment and simulations is in the plasma potential. In this case, three measurements are available along the axis. These measurements show a flat or slightly increasing trend in the plasma potential as we move upstream in the cathode tube while our simulations suggest a decreasing trend. The electron temperature, on the other hand, suggests a decreasing trend for both experiment and simulation. From Ohm's law, the plasma potential is approximately proportional to the product of the electron temperature and density in the absence of large electron currents and resistivity. The latter quantities should become smaller the more upstream we move in the tube as most of the electron current is generated relatively close to the orifice plate. Since both plasma density and electron temperature are decreasing as shown in Fig. 3, a decreasing trend in the plasma potential would be expected as we move upstream in the cathode tube. A decreasing trend in the plasma potential has also been found in other cathodes examined with OrCa2D that agreed with experimental measurements, for instance [8-9,11]. Thus, we conclude that the plasma potential measurements carry a larger uncertainty than the error bars below indicate and that overall the comparison between numerical simulation results and measurements is satisfactory.

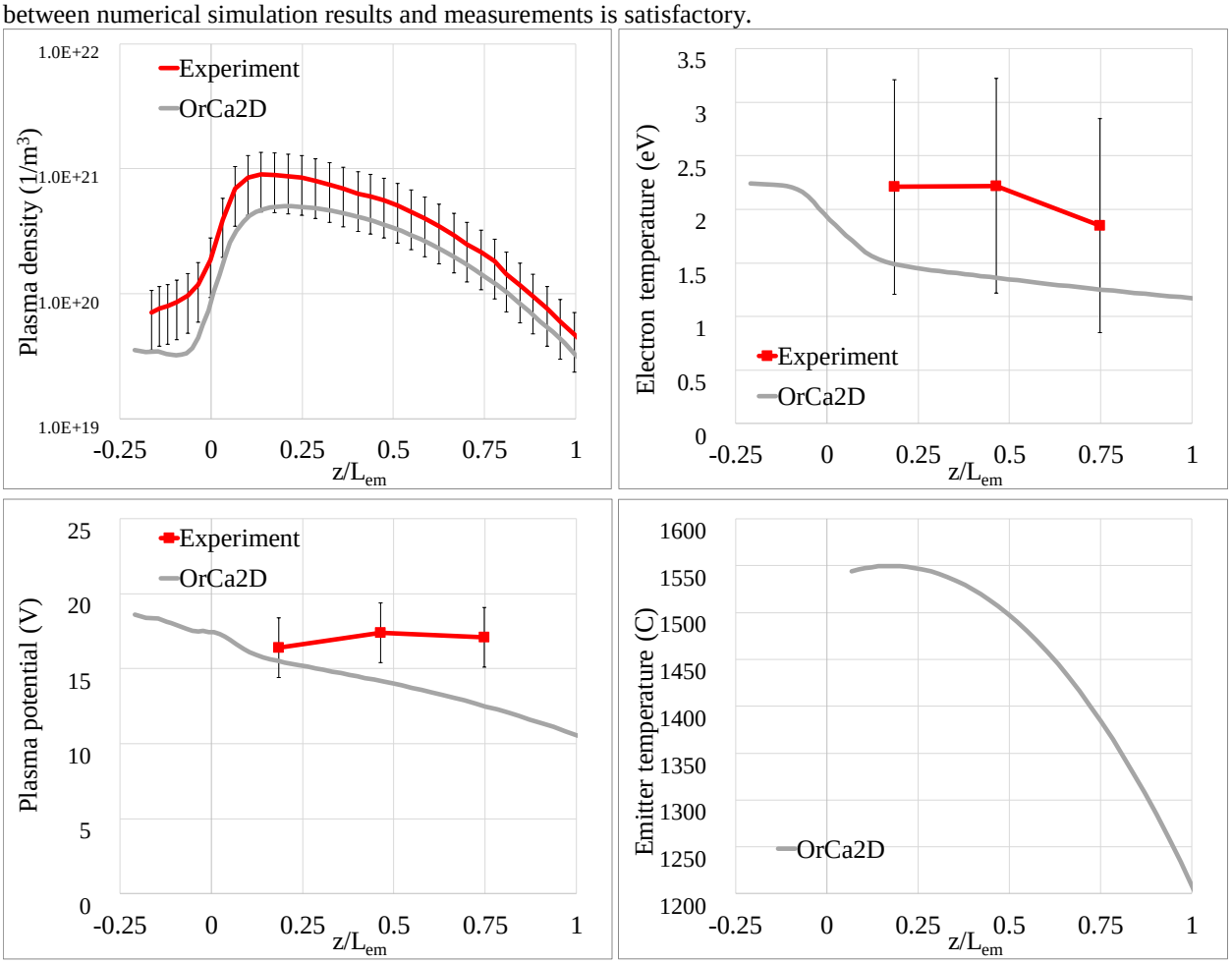

Figure 3. Comparison between internal plasma measurements and OrCa2D numerical simulation results along the cathode centerline and along the emitter surface for the LaB_6 cathode with nominal diameter. Simulation run with mass flow rate of 14.8 sccm (compared to 13.1 sccm for the measurements) and discharge current of 25 A. Top-left: plasma density, top-right: electron temperature, bottom-left: plasma potential, bottom-right: emitter temperature (no reliable measurements exist for this configuration/operating condition).

B. Comparison between numerical results and experimental measurements in the BaO cathode

As in the case of the LaB_6 cathode, two orifice diameters (nominal and 40% smaller-than-nominal diameter) were proposed. The cathode with the nominal orifice diameter was ultimately selected since, as shown in Fig. 4, larger orifices typically lead to lower emitter temperatures under the same operating condition. Larger orifices produce a

more even distribution of the plasma along the length of the emitter, avoiding large plasma density peaks close to the orifice plate. This in turn leads to lower thermal loads in the downstream end of the emitter, where the emitter temperature reaches its maximum value. Reliable emitter temperature measurements were achieved for the BaO cathode and were used to prescribe the profiles needed as input by OrCa2D. In addition, internal measurements of the plasma density were obtained for the two cathodes operating at the nominal condition of 7% anode flow rate (14.8 sccm, 1.4 mg/s) and discharge current of 20.8 A. However, the measurements for the cathode with nominal orifice were not reliable as they exhibited an unexpectedly flat density profile, with an average value that was an order of magnitude lower than the average density inside the cathode with the lower-than-nominal orifice diameter. We have also found that no reasonable emitter temperature profile can lead to such uncharacteristically flat plasma density distribution along the cathode centerline. Thus, no direct comparison between simulation and measurement could be made for the nominal BaO cathode. However, we can make these comparisons in the cathode with the smaller orifice and draw some conclusions for the larger orifice cathode. In Fig 4, we show the comparison between the computed and measured plasma density (the only measurement available). Simulation results for both orifice sizes agree extremely well with the measurement for the BaO cathode with small orifice diameter except downstream of the orifice (outside the cathode tube). This discrepancy is largely due to the different magnetic fields used in the simulation and experiment. The experiment was performed with a coil that produced a magnetic field whose spatial variation only approximated that of HERMeS whereas the OrCa2D simulations use the actual field produced by the thruster's magnetic circuit. The ratio between the maximum magnitude of the field along the cathode centerline for the HERMeS thruster at the nominal $B_{r,max}$ over that in the test was 2.8. Consequently, the plasma density exhibits a higher peak value in the simulation, since increasing the strength of the magnetic field increases plasma confinement along the centerline. This result does not contradict in principle the assumption that the same emitter temperature profile can be used for different magnetic field strengths at the same operating condition, since changes in the plasma parameters due to the magnetic field are found outside of the cathode tube and in the downstream-most 5% of the tube. The plasma density profile is obtained using an emitter temperature distribution along the axis that closely resembles the measurements. For the nominal cathode, no measurement of the plasma density is available. The computed density profile however is found to be not very different from that obtained in the cathode with the small orifice, except for a lower value of the maximum plasma density (a well-known feature of increasing the orifice diameter). The emitter temperature for the nominal cathode is lower than for the small-orifice cathode (also a well-known consequence of increasing the orifice diameter). Regarding the accuracy of our numerical results for the nominal cathode, in light of the absence of plasma measurements, we argue that the density distribution in numerical simulations for both cathodes was obtained using the measured emitter temperature. This approach produced excellent agreement with measurements for the small-orifice cathode and both cathodes share emission properties and internal geometry. Thus, we find no reason to believe that the computed plasma density for the nominal cathode should be significantly different from the measured density in the same arrangement that was simulated (if such measurement existed).

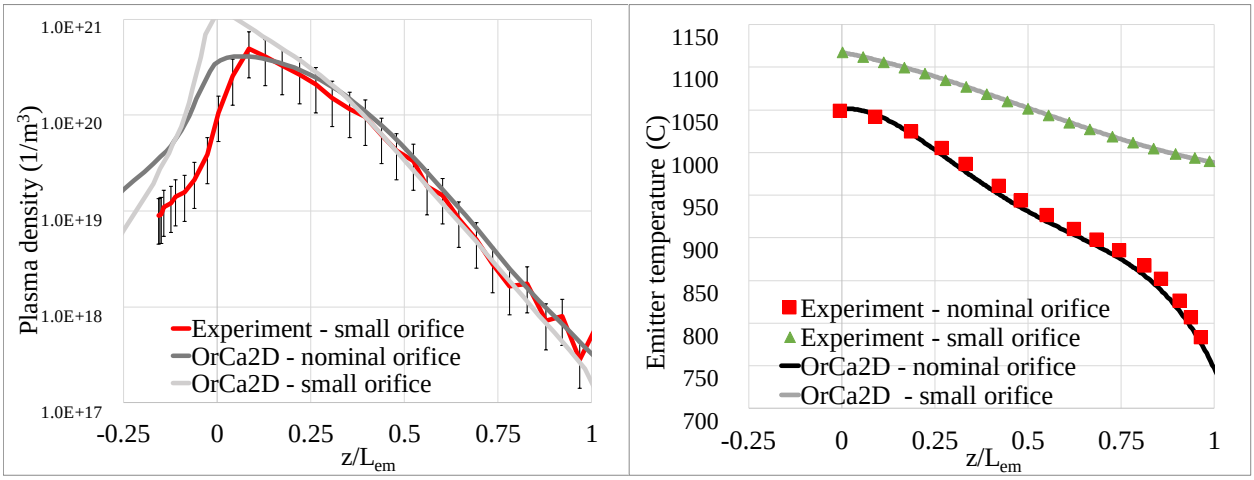

Figure 4. Comparison between internal plasma measurements and OrCa2D numerical simulation results along the cathode centerline and along the emitter surface for the BaO cathodes. Experiment and simulation run with mass flow rate of 1.4mg/s (14.8 sccm) and discharge current of 20.8 A. Top-left: plasma density, top-right: emitter temperature.

IV. Life assessment of the BaO and LaB_6 cathodes for HERMeS

This section summarizes the results of the parametric study we conducted to determine whether the two proposed cathode technologies can meet the service lifetime requirements of HERMeS. As a decision has been made to use the nominal BaO cathode in the EDU currently being manufactured by Aerojet-Rocketdyne for AEPS, the parametric study is more extensive for the BaO cathode than for the LaB_6 cathode, and includes all possible $B_{r,max}$, cathode flow rates, and the low-power condition (9 A). Only selected cases are presented for the LaB_6 cathodes. In the case of the low-power condition, emitter temperature measurements were available but plasma measurements were not. We performed all our simulations for the 9-A condition using the measured emitter temperature profile as input, in light of results in Section III B which exhibited good agreement with the measured plasma density when the measured emitter temperature was used in the simulations for other operating conditions.

A. Emitter life

Emitter life is largely driven by temperature. As suggested by [7], we can use the following empirical relations for LaB_6 and BaO emitters, respectively to determine their operational life:

$$t_{em}(\text{kh}) = 2.24\cdot 10^{16} h_{em}(\mu\text{m}) \exp\left(-0.0257 T_{em}(^{\circ}\text{C})\right), \quad (1)$$

$$t_{em}(\text{kh}) = \frac{1}{1000}\left(\frac{h_{em}(\mu\text{m})}{100}\right)^2 \exp\left(\frac{3.2777}{T_{em}(^{\circ}\text{C})}\cdot 10^4 - 15.488\right), \quad (2)$$

where t_{em} is the emitter lifetime, h_{em} is the emitter thickness, and T_{em} is the emitter temperature.

The maximum emitter temperatures and the expected life associated to them are summarized in Table I. Following the extrapolation rules summarized in Section III, the BaO cathode simulations for the same discharge current and varying magnetic field and/or mass flow rate employ the same emitter temperature profile. As expected, the emitter temperature for the BaO cathode operating at 9 A is lower than the temperature achieved for the 20.8-A condition. LaB_6 cathodes operate at a higher temperature than BaO cathodes but their expected life for a given temperature is higher. Results for both BaO and LaB_6 cathodes greatly exceed the requirements of the HERMeS thruster (34.5 kh, including the 50% margin). Even though no simulations were run with the LaB_6 cathodes at the low-power condition, we can argue that, since lower discharge currents result in lower emitter temperatures, emitter life would not be a cause for concern for the LaB_6 cathodes operating at a 9-A discharge current.

Table I. Maximum emitter temperature and expected life based on Eqs. (1-2)

Cathode	Discharge current (A)	Max emitter temperature (C)	Expected life (kh)
BaO nominal orifice	**9**	970	$22.3\text{x}10^3$
	20.8	1035	$5.8\text{x}10^3$
	23	1050	$4.5\text{x}10^3$
LaB6 nominal orifice	**25**	1560	$1.35\text{x}10^2$
LaB6 50% larger-than-nominal orifice	**25**	1582	$6.6\text{x}10^1$

B. Erosion in the LaB_6 cathode

Using results from the plasma simuilations, we compute the erosion rate due to ion sputtering of a surface using the relation

$$\varepsilon = j_i Y(K_i), \tag{3}$$

where ε is the erosion rate, j_i the ion current density at the surface, and Y the sputtering yield (Fig. 5) defined as a function of the energy of the ions at the surface K_i. The orifice plate is made of tungsten and the keeper is made of graphite.

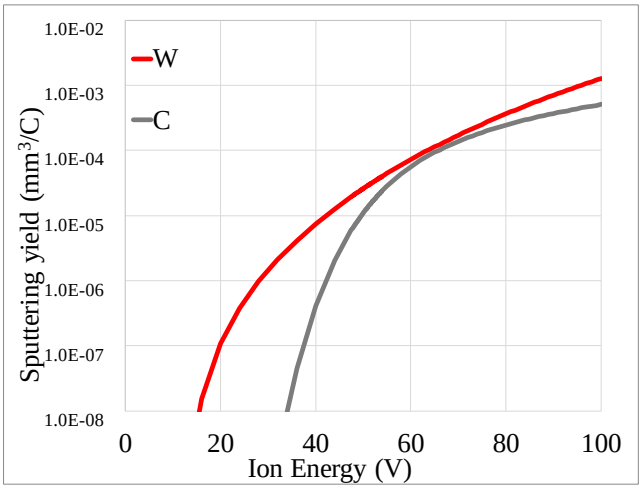

Figure 5. Sputtering yield as a function of ion energy for tungsten (W) and graphite (C)

A summary of the maximum erosion rates at the orifice plate and keeper of the LaB_6 cathodes is presented in Table II. The discharge current in these simulations is 25 A, which is the condition that was compared with experiments (Section III), and higher than the nominal condition of 20.8 A. A higher-than-nominal current was used to emulate the peak current attained during the thruster's discharge current oscillations. Keeper erosion is negligible due to the sputtering threshold for graphite being approximately 40 V. The latter value being two times the discharge voltage, it is extremely unlikely that singly charged ions with such large kinetic energy exist for the conditions at which the cathode is operated. We have evidence that mechanisms that produce high-energy ions can be present in hollow cathodes. It was discussed in the introduction that plume mode, characterized by large global oscillations in the discharge, can produce high energy ions in the plume that in turn lead to enhanced erosion rates. Plume mode typically occurs at low-current conditions and mass flow rates. However, to date, performance and long-duration testing performed at JPL and GRC has revealed no indications that operation at the 9-A or 20.8-A conditions have been detrimental to cathode health for any of the cathodes. High-energy ions can also be generated due to the heating process associated with the ion-acoustic turbulence in the cathode plume. Our most recent model [18,19] accounts for this phenomenon and has found moderate heating (in the order of 1 to 2 eV) for the operating envelope required by HERMeS.

Erosion rates of the orifice plate are not negligible but extremely small (of the order of 10^{-3} mm/kh for the cathode with nominal orifice diameter and 10^{-4} mm/kh for the cathode with the large orifice diameter). As explained in previous work [e.g. 12], an increased erosion rate for the cathode with a narrower orifice is expected since the electron current density would increase, which would lead to a larger resistive drop across the orifice and, consequently to higher sheath energy for the ions. The plasma density would also increase which would lead to higher ion flux to the walls. Erosion rates also slightly increase when a magnetic field is applied as the plasma becomes more confined around the thruster centerline. Based on these results we estimate that after 34.5 kh, the orifice plate will have a maximum erosion of 0.06 mm. This is a highly conservative estimate since we know that as the orifice widens the erosion rate decreases [e.g. see 12]. Thus, orifice plate erosion in the LaB_6 cathode is not expected to be a cause for failure since geometry changes in the cathode will be minimal over its life. The 9-A case has not been investigated, but based on the decreased current density expected when the thruster operates at a lower discharge current and experience with other cathodes (see Table III), we do not anticipate larger erosion rates at the low-current condition.

Table II. Erosion rates for the LaB_6 cathodes (CFF=cathode flow fraction)

EROSION RATE (mm/kh)	LaB_6 nominal orifice I_d=25 A 7% CFF (1.4 mg/s) V_d=20 V		LaB_6 large orifice I_d=25 A 7% CFF (1.4 mg/s) V_d=23 V	
Br_{max} at Discharge Channel CL	Orifice $\times 10^{-3}$	Keeper $\times 10^{-3}$	Orifice $\times 10^{-3}$	Keeper $\times 10^{-3}$
0 G	1.04	0	0.05	0
75 %Nominal	1.75	0	0.07	0

C. Erosion in the BaO cathode

Erosion of the nominal BaO cathode surfaces was computed using Eq. (3) and the same sputtering yield functions employed in the analysis of the LaB_6 cathodes. Since this cathode has been selected for implementation in the EDU, we explore here the full range of operating conditions for this cathode. We also include a higher-than-nominal condition (23 A) that accounts for the demands of higher currents from the cathode during thruster oscillations. Table III and IV summarize results for the orifice plate and keeper, respectively. Keeper erosion due to singly charged cathode ions is, as in the case of the LaB_6 cathodes, negligible due to the high sputtering threshold for graphite. With respect to orifice plate erosion, we observe large homogeneity in the results with varying magnetic field. This is expected as the Hall parameter at the orifice is relatively small (between 0.5 and 3). In consequence, increasing the magnetic field by less than a factor of two does not alter significantly the plasma in the orifice region. Larger differences are typically noticed between the results with and without applied magnetic field (for instance, see Table II). Erosion rates tend to increase by a factor of between two and three when decreasing the mass flow rate below 7%. Decreasing the mass flow rate for a given discharge current produces an increase in the discharge voltage, which in turn results in ions with higher energies in the orifice region. The erosion rate, as expected, increases with discharge current. For the higher-than-nominal case, the two effects described above are combined: the current is higher but also the mass flow rate relative to the discharge current is lower. With these results, the maximum erosion of the orifice plate after 34.5 kh is 0.01 mm. As in the LaB_6 case, orifice plate erosion is not a cause for concern.

Table III. Maximum erosion rate of the orifice plate in the nominal BaO cathode at multiple operating conditions (CFF=cathode flow fraction)

EROSION RATE (mm/kh)	I_d=9 A			I_d=20.8 A			I_d=23 A
Br_{max} at Discharge Channel CL	5% CFF (0.43 mg/s) V_d=19.9 V $\times 10^{-3}$	7% CFF (0.61 mg/s) V_d=16.1 V $\times 10^{-3}$	9% CFF (0.78 mg/s) V_d=15.5 V $\times 10^{-3}$	5% CFF (1.0 mg/s) V_d=15.5 V $\times 10^{-3}$	7% CFF (1.4 mg/s) V_d=13.4 V $\times 10^{-3}$	9% CFF (1.9 mg/s) V_d=13.0 V $\times 10^{-3}$	7% CFF (1.4 mg/s) V_d=14.6 V $\times 10^{-3}$
75% Nominal	-	-	-	0.08	0.04	0.04	0.34
Nominal	0.03	0.01	0.01	0.09	0.04	0.04	-
125% Nominal	-	-	-	0.07	0.03	0.04	-

Table IV. Maximum erosion rate of the keeper electrode in the nominal BaO cathode at multiple operating conditions from OrCa2D simulation results (CFF=cathode flow fraction)

EROSION RATE (mm/kh)	I_d=9 A			I_d=20.8 A			I_d=23 A
Br_{max} at Discharge Channel CL	5% CFF (0.43 mg/s) V_d=19.9 V $\times 10^{-3}$	7% CFF (0.61 mg/s) V_d=16.1 V $\times 10^{-3}$	9% CFF (0.78 mg/s) V_d=15.5 V $\times 10^{-3}$	5% CFF (1.0 mg/s) V_d=15.5 V $\times 10^{-3}$	7% CFF (1.4 mg/s) V_d=13.4 V $\times 10^{-3}$	9% CFF (1.9 mg/s) V_d=13.0 V $\times 10^{-3}$	7% CFF (1.4 mg/s) V_d=14.6 V $\times 10^{-3}$
75% Nominal	-	-	-	0	0	0	0
Nominal	0	0	0	0	0	0	-
125% Nominal	-	-	-	0	0	0	-

D. Erosion of the keeper due to thruster ions using Hall2De

OrCa2D's development in early 2000 began with the objective to capture only processes in the cathode interior where the ionization rates for multiply charged ions are negligible [8]. Therefore, only singly charged ions were included in those early versions of the code. Soon thereafter OrCa2D was extended to include also the plume region of the cathode [11] where the concentration of doubly and triply charged ions remains, typically, considerably lower than those of singly charged ions, but may become high enough in some cases that their contribution to the erosion of the keeper is not negligible. This is because these ions have energies that are twice or thrice higher than those of singly charged ions. Because OrCa2D does not account for sputtering by multiply-charged ions or ions generated by the Hall thruster, erosion of the keeper electrode by these processes required the support of Hall2De.

In our companion paper [29], we present erosion rate predictions for the thruster channel walls and pole covers. Hall2De was designed to include in the computational domain the actual thruster geometry, including the exact location of the cathode with respect to the thruster. Hall2De models the keeper orifice exit as a single edge at which the cathode mass flow rate is imposed. Ionization (up to Xe_{3+} state) in the cathode plume is self-consistently computed based on the plasma parameters in the region (such as density and electron temperature). The keeper surface is discretized by two or three boundary edges, enabling erosion computations at them. However, due to computational constraints, the computational grid in the cathode plume region is not as refined as in OrCa2D. Moreover, because the cathode interior plasma is not self-consistently coupled to the exterior plasma, boundary conditions for the electron temperature, plasma potential and ion to neutral flux fractions must be imposed and are based on assumed values. Consequently, compared to more resolved, cathode-thruster fully coupled simulations, the numerical results cannot be as accurate. Hall2De uses a mixed fluid/particle-in-cell (PIC) approach to model ions in a Hall thruster. Ions generated in the channel and cathode plume are modeled with a multi-fluid algorithm. Ions generated in the plume and acceleration regions are modeled with PIC due to the wide range of ion energies found, which makes fluid averaging inaccurate for erosion computations. Further details can be found in [29].

Table V summarizes the maximum erosion rates at the keeper surface (note that Hall2De results are independent of the type of cathode used) due to contribution of all the ions populations included in Hall2De. We show results for the nominal operating condition of 600 V – 20.8 A. Two relative positions of the cathode with respect to the thruster were considered. In the "cathode upstream" configuration, the keeper surface facing the cathode plume is more upstream (in the axial direction) than the pole cover. In the second configuration, "cathode downstream", the keeper surface in on the same plane as the inner pole cover (Fig. 6). Erosion due to singly charged cathode ions (ions generated in the cathode plume) is negligible for both cathode locations. This result is consistent with OrCa2D simulations, which did not show any erosion due to singly charged ions (their energies being below the sputtering threshold for graphite). We observe, however, erosion due to thruster ions (ions generated in the thruster channel, acceleration region, or thruster plume) that accounts for 50% or more of the total erosion in all the cases examined. The erosion rates at the keeper are comparable to those found in the inner pole cover [29]. For the nominal magnetic field strength condition, for which numerical results in the two configurations are available, the erosion rate due to thruster ions in

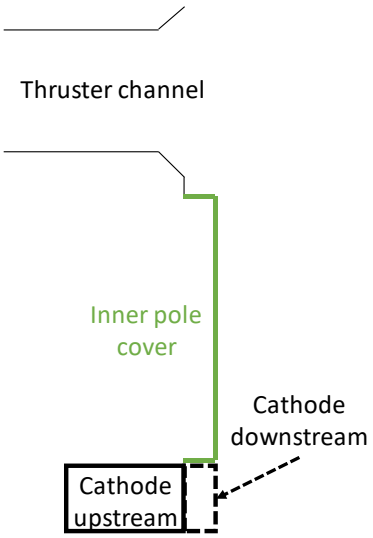

Figure 6. Schematic of cathode locations with respect to inner pole cover

the "cathode downstream" configuration is twice as high as the erosion rate in the "cathode upstream" configuration. This can be attributed to the pole cover in the "cathode upstream" configuration providing some shielding from ions originating close to the channel. The erosion due to thruster ions also appears to increase with applied magnetic field, an effect also noticed for the inner pole erosion at 600 V [29]. This trend is related to higher values of the plume plasma potential occurring at higher $B_{r,max}$, a phenomenon that leads to increased sheath potentials (and ion energies at the surface).

An important factor to consider in the uncertainty of the estimates of erosion due to thruster ions is the modeling of angular momentum for ions being simulated by PIC. In the PIC algorithm, the angular momentum is a constant of motion: $r_0 u_{\theta,0} = r u_\theta$, where the 0 subscript denotes the conditions when the particle was generated and u_θ is the azimuthal velocity. $u_{\theta,0}$ is proportional to the square root of the ion temperature. As the ions approach the thruster centerline, conservation of angular momentum becomes more relevant. The azimuthal component of the velocity increases, which affects the velocity in the radial direction. The latter decreases and ultimately gets its direction reversed, preventing them from reaching the centerline. If the ion temperature increases (and subsequently the angular momentum), ions reverse trajectories further away from the centerline, resulting in less ions sputtering the keeper surface. Results shown in Table V are for "cold ions" (0.07 eV), which is a worst-case estimate for the erosion. In Fig. 7, we show for completion a comparison of the erosion rate at the keeper when the temperature of the ions is increased to 6 eV (approximately 10% of the axial velocity of the ions). We observe that the current density of thruster ions decreases very steeply at the keeper surface when ions are warm, lowering the erosion rate proportionally. Hall2De simulations also show, in some cases, erosion due to doubly and triply charged ions. At most, their contribution to the erosion is similar to that of thruster ions. We consider these estimates only qualitative however due to the coarse resolution of the grid in the plume region and the high sensitivity of the sputtering yield for ions energies similar to the sputtering threshold (~40 V for carbon). For instance, the erosion rate for doubly and triply charged ions in the downstream configuration at the nominal $B_{r,max}$ is reported as negligible while for the cathode upstream configuration is comparable to that of thruster ions. These differences between configurations are due to the sheath potential, which accounts for a large fraction of the energy of cathode ions that sputter the keeper, having a lower value in the downstream configuration. We have found that moving the location of the cathode downstream leads to lower plasma potential values in the cathode plume (Fig. 8). This is due to a reduction of the Hall parameter as the plasma density moves downstream while the magnetic field stays fixed. Thus, lower erosion rates due to cathode ions are expected in the downstream configuration. However, the uncertainty in the exact value of the sheath potential may lead to significant changes in the erosion rate when a difference of 2-3 V can put the energy of the ions below or above the sputtering threshold.

Table V. Maximum erosion rates at the keeper surface from Hall2De simulations that include multiply charged ions and ions generated in the thruster channel and plume

EROSION RATE (mm/kh)	**V_d=600 V, I_d=20.8 A Cathode Upstream**					**V_d=600 V, I_d=20.8 A Cathode Downstream**				
Br_{max} at Discharge Channel CL	**Thruster ions** $\times 10^{-3}$	**Cathode Ions (Xe+)** $\times 10^{-3}$	**Cathode ions (Xe2+)** $\times 10^{-3}$	**Cathode ions (Xe3+)** $\times 10^{-3}$	**Total** $\times 10^{-3}$	**Thruster ions** $\times 10^{-3}$	**Cathode ions (Xe+)** $\times 10^{-3}$	**Cathode ions (Xe2+)** $\times 10^{-3}$	**Cathode ions (Xe3+)** $\times 10^{-3}$	**Total** $\times 10^{-3}$
75% Nominal	50	0	21	49	120	-	-	-	-	-
Nominal	45	0	14	23	81	85	0	0	0.04	85
125% Nominal	140	0	0.7	18	150	-	-	-	-	-

Based on the nominal operating condition for HERMeS (600 V, 20.8 A, nominal $B_{r,max}$) and 34.5 kh of operation, the erosion rates computed by Hall2De when the cathode is in its upstream location suggest that the keeper surface may erode by as much as 1.6 mm due to bombardment by thruster ions, and almost twice this value if the (less accurately estimated) contribution of multiply charged ions is included. Even higher erosion is expected if the thruster is operated at the higher magnetic field for the same time. It should be noted that these results most likely constitute a conservative estimate due to the assumption of "cold ions". Nevertheless, the HERMeS development team has taken action to tackle this risk by increasing the keeper thickness and by baselining the cathode-upstream configuration. To further reduce risk, there are also plans for further wear testing and modeling of the cathode keeper erosion to more accurately determine the erosion rates at multiple operating conditions.

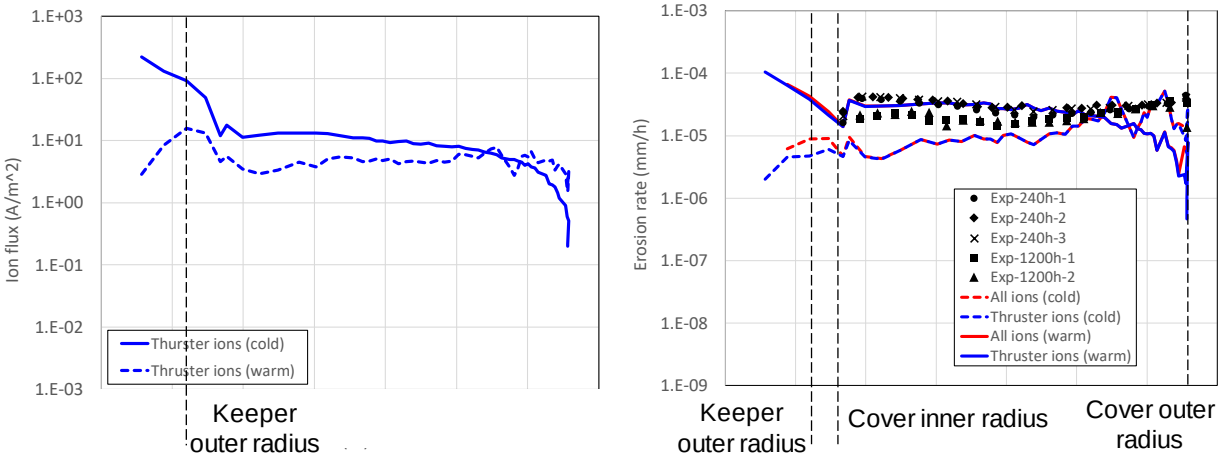

Figure 7. Ion current density and erosion rate of thruster ions under the assumption of "cold" and "warm" ions showing the sensitivity of the erosion results on the angular momentum of PIC ions. Symbols in the right figure denote erosion rates from the TDU-1 wear test at 600 V – 20.8 A after 240 and 1200 hours [32].

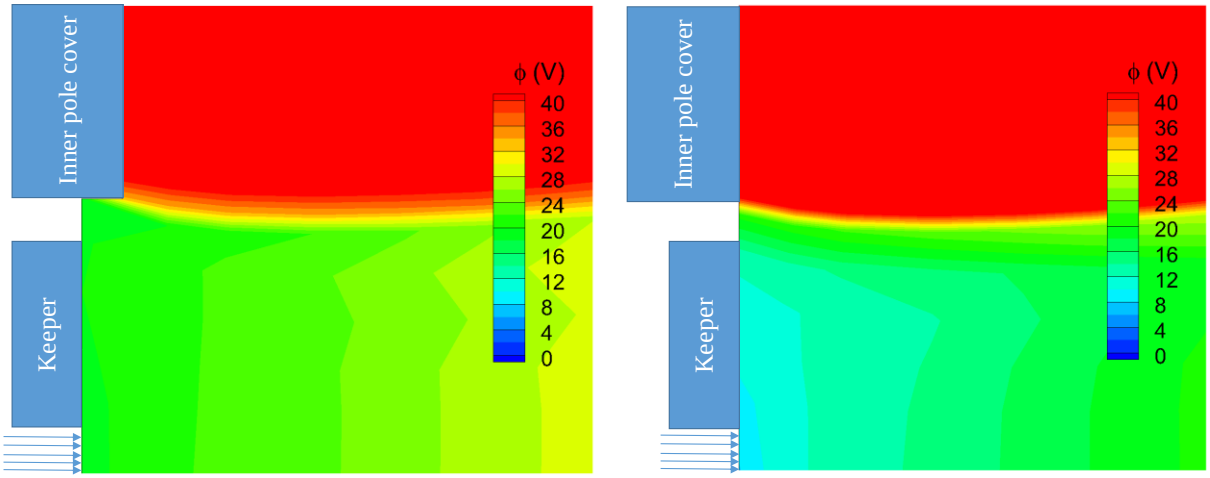

Figure 8. 2-D plasma potential contours near the keeper for cathode upstream (left) and downstream (right) configurations in Hall2De simulations.

V. Conclusion

We have performed a detailed numerical analysis of the LaB_6 and BaO cathodes proposed for HERMeS, with the objective of assessing the impact of known failure mechanisms in these devices during operation of the thruster for 34.5 kh. The failure mechanisms that have been investigated in this work are depletion/vaporization of the emitter material, and erosion of the cathode plate and keeper electrode. The numerical simulations were performed with the

OrCa2D code, with support from Hall2De simulations in the determination of keeper erosion. OrCa2D results were compared to internal plasma measurements and emitter temperature data in cases for which such data were available.

The range of emitter temperatures found in the operating envelope of the cathode suggest emitter life that greatly exceeds the requirement of 34.5 kh of operation for both emitters. For the baseline (BaO) cathode, emitter life is expected to exceed 4,500 kh. The worst case found exhibits a margin of 100% with respect to the latter figure. Values found for orifice erosion are extremely small, with erosion depths of less than 0.1 mm in all cases.

Finally, we found that in its current configuration erosion of the keeper electrode is large enough that it does not meet the life requirement plus margin. The erosion is due, largely, to sputtering by thruster ions. These ions are generated inside the acceleration channel or in the thruster plume and erode the keeper in the same manner they erode the inner front pole cover of the thruster. In response of these results and experimental measurements that confirm the trends found in simulations [32], the HERMeS development team has taken the action to increase the keeper thickness and place the cathode upstream of the pole cover surface (facing the plasma) in a way that the latter shields partially the keeper from thruster ions.

Acknowledgments

The research described in this paper was carried out by the Jet Propulsion Laboratory, California Institute of Technology, under a contract with the National Aeronautics and Space Administration. The support of the joint NASA GRC and JPL development of the Advanced Electric Propulsion System by NASA's Space Technology Mission Directorate through the Solar Electric Propulsion Technology Demonstration Mission project is gratefully acknowledged.

References

[1] Hofer, R. R., Polk, J. E., Sekerak, M. J., Mikellides, I. G., Kamhawi, H., Sever-Verhey, T. R., Herman, D. A., and Williams, G., "The 12.5 kW Hall Effect Rocket with Magnetic Shielding (HERMeS) for the Asteroid Redirect Robotic Mission", AIAA paper 2016-4825, July 2016.

[2] Brophy, J. R., and Friedman, L., "Returning an Entire Near-Earth Asteroid in Support of Human Exploration Beyond Low-Earth Orbit," in IAF Global Exploration Conference, Washington, D. C., 2012.

[3] Brophy, J. R., Friedman, L., and Culick, F., "Asteroid Retrieval Feasibility," in Aerospace Conference, 2012, Big Sky, MT, 2012, pp. 1 - 16.

[4] Brophy, J. R., and Oleson, S., "Spacecraft Conceptual Design for Returning Entire Near-Earth Asteroids", AIAA paper 2012-4067, July 2012.

[5] Herman, D., Tofil, T., Santiago, W., Kamhawi, H., Mcguire, M., Polk, J. E., Snyder, J. S., Hofer, R., Picha, F., Jackson, J., and Allen, M., "Overview of the Development and Mission Application of the Advanced Electric Propulsion System (AEPS)," IEPC-2017-284, October 2017.

[6] Hofer, R. and Kamhawi, H., "Development Status of a 12.5 kW Hall Thruster for the Asteroid Redirect Robotic Mission," IEPC-2017-231, October 2017.

[7] Goebel, D. M., and Katz, I., *Fundamentals of Electric Propulsion*, JPL Space and Technology Series, Jet Propulsion Laboratory, California Institute of Technology, 2008.

[8] Mikellides, I. G., Katz, I., D. Goebel, D. M., and Polk, J. E., "Hollow Cathode Theory and Experiment II: A Two-dimensional Theoretical Model of the Emitter Region", *Journal of Applied Physics*, Vol. 98, No. 11, 2005, 113303, doi: 10.1063/1.2135409

[9] Mikellides, I. G, Katz, I., Jameson, K. K., and Goebel, D. M., "Numerical Simulations of a Hall Thruster Hollow Cathode Plasma", IEPC-2015-018, in proceedings of the 30th International Electric Propulsion Conference, Florence, Italy, September 2007.

[10] Mikellides, I. G., Katz, I., Goebel, D. M., Jameson, K. K. and Polk, J. E., "Wear Mechanisms in Electron Sources for Ion Propulsion II: Discharge Hollow Cathodes", *Journal of Propulsion of Power*, Vol. 24, No 4, 2008, 866-879, doi: 10.2514/1.33462

[11] Mikellides, I. G., Katz, I., Goebel, D. M., Polk, J. E., and Jameson, K. K., "Evidence of Non-classical Plasma Transport in Hollow Cathodes for Electric Propulsion", *Journal of Applied Physics*, Vol. 101, No. 6, 2007, 063301, doi: 10.1063/1.2710763

[12] Mikellides, I. G. and Katz, I., "Wear Mechanisms in Electron Sources for Ion Propulsion I: Neutralizer Hollow Cathode", *Journal of Propulsion and Power*, Vol. 24, No. 4, 2008, 855-865, doi: 10.2514/1.33461

[13] Mikellides, I. G., Goebel, D. M., Jorns, B. A., Polk, J. E., and Guerrero, P., "Numerical Simulations of the Partially-ionized Gas in a 100-A LaB6 Hollow Cathode", *IEEE Transactions on Plasma Science, Special Issue on Plasma Propulsion*, Vol. 43, No. 1, 2015, pp. 173-184, doi: 10.1109/TPS.2014.2320876

[14] Polk, J. E., Anderson, J. R., Brophy, J. R., Rawlin, V. K., Patterson, M. J., Sovey, J., and Hamley, J., "An Overview of the Results from an 8200 Hour Wear Test of the NSTAR Ion Thruster," AIAA paper 99-2446, June 1999.

[15] Sengupta, A., Brophy, J. R., and Goodfellow, K. D., "Status of the Extended Life Test of the Deep Space I Flight Spare Ion Engine after 30,352 Hours of Operation", AIAA paper 03-4558, July 2003.
[16] Jorns, B. A., Mikellides, I. G., and Goebel, D. M., "Ion Acoustic Turbulence in a 100-A LaB6 Hollow Cathode", Physical Review E, Vol. 90, 2014, 063106, doi: 10.1103/PhysRevE.90.063106
[17] Jorns, B. A., Mikellides, I. G., Goebel, D. M., and Lopez Ortega, A., "Mitigation of Energetic Ions and Keeper Erosion in a High-current Hollow Cathode", IEPC-2015-134, in proceedings of the 34th International Electric Propulsion Conference, Hyogo-Kobe, Japan, July 2015
[18] Lopez Ortega, A., Mikellides, I. G., and Jorns, B. A., "First-principles Modeling of IAT-driven Anomalous Resistivity in Hollow Cathode Discharges II: Numerical Simulations and Comparisons with Experiments", AIAA paper No. 2016-4627, July 2016.
[19] Lopez Ortega, A., Mikellides, I. G., and Jorns, B. A., "Hollow Cathode Plasma Simulations with a First-principles Model of IAT-driven Anomalous Resistivity", submitted to *Journal of Propulsion and Power*, 2017.
[20] Mikellides, I. G., Katz, I., Goebel, D. M., and Polk, J. E., "Theoretical Model of a Hollow Cathode Insert Plasma", AIAA paper No. 2004-3817, July 2004.
[21] Bychenkov, V. Y., Silin, V. P., and Uryupin, S. A., "Ion-acoustic Turbulence and Anomalous Transport", *Physics Reports*, Vol. 164, Issue 3, 1988, 199-215, doi: 10.1016/0370-1573(90)90122-I
[22] de Kluvier, H., Perepelkin, N. F., and Hirose, A., "Experimental Results on Current-driven Turbulent Plasmas – a Survey", *Physics Reports*, Vol. 199, Issue 6, 1991, 281-381, doi: 10.1016/0370-1573(91)90060-Y
[23] Stix, T. H., *Waves in Plasmas*, Springer-Verlag, New York, 1992.
[24] Horton, H., *Turbulent transport in magnetized plasmas*, World Scientific, Singapore, 2012.
[25] Marchand, R. and Dumberry, M., "CARRE: a Quasi-orthogonal Mesh Generator for 2D edge Plasma Modelling", *Computer Physics Communications*, Vol. 96, 1996, pp. 232-246, doi: 10.1016/0010-4655(96)00052-5
[26] Lin, Z., Hahm, T. S., Lee, W. W., Tang, W. M., and White, R. B., "Turbulent Transport Reduction by Zonal Flows: Massively Parallel Simulations," *Science*, Vol. 281, 1998, pp. 1835-1837, doi: 10.1126/science.281.5384.1835
[27] Dusham, S., "Electron Emission from Metals as a Function of Temperature", *Physical Review*, Vol. 21, No. 6, 1923, 623-636, doi:10.1103/PhysRev.23.153
[28] Mikellides, I. G., Goebel, D. M., Snyder, J. S., Katz, I., and Herman, D. A., "The Discharge Plasma in Ion Engine Neutralizers: Numerical Simulations and Comparisons with Laboratory Data," *Journal of Applied Physics*, Vol. 108, No. 11, 2010, pp. 113308 (1-12).
[29] Lopez Ortega, A., Mikellides, I. G., and Chaplin, V. H., "Simulations for the Assessment of Pole Erosion in the 12.5-kW Hall Effect Rocket with Magnetic Shielding (HERMeS), IEPC paper 2017-154, October 2017.
[30] Polk, J. E., Grubisic, A., Taheri, N., and Hornbeck, S., "Emitter Temperature Distributions in the NSTAR Discharge Hollow Cathode", AIAA paper 2005-xx, July 2005.
[31] Polk, J. E., Goebel, D. M., and Guerrero, P., "Thermal Characteristics of a Lanthanum Hexaboride Hollow Cathode", IEPC paper 2015-44, July 2015.
[32] Williams, G., Gilland, J. H., Kamhawi, H., Choi, M., Peterson, P. Y., and Herman, D., "Wear Trends of the HERMeS Thruster as a Function of Throttle Point," IEPC-2017-207, October 2017.